

Towards Achieving Sustainability in Additive Friction Stir Deposition



Sweta Baruah, Joshua Hoekstra, Madelyn Carter, Rob Patterson,
Brett Compton, and Tony Schmitz

Abstract Additive friction stir deposition (AFSD) uses a non-consumable rotating tool to generate frictional heat and plastic deformation, allowing metals to be deposited layer by layer onto a substrate without melting. This solid-state process offers a unique opportunity for upcycling metallic chips produced as waste from machining operations to produce feedstock bars due to its high degree of tolerance for feed material quality. Accordingly, this work presents a chip compactor design integrated into a hydraulic press and comprising a die set and ram carriage assembly. The application of controlled compressive mechanical forces under both cold and warm working conditions enables the compactor system to produce aluminum (Al 6061) feedstock bars from machining chips with 86–100% density relative to wrought Al 6061. Compacted bars were also obtained using shredded Al can waste and a composite mixture of 25% low-cost SiC powder with machined Al chips. Optical microscopy characterization results of these compacted bars are presented here. These upcycled compacted bars are then used as feedstock material for AFSD, contributing towards achieving sustainability in additive manufacturing in general by adopting a circular economy model.

Keywords Additive friction stir deposition · Solid-state additive manufacturing · Metal recycling · Sustainability · Circular economy

S. Baruah (✉) · J. Hoekstra · R. Patterson · B. Compton · T. Schmitz
Mechanical, Aerospace, and Biomedical Engineering, University of Tennessee, Knoxville, TN,
USA
e-mail: sbaruah@utk.edu

M. Carter
Roane State Community College, Harriman, TN, USA

T. Schmitz
Manufacturing Demonstration Facility, Oak Ridge National Laboratory, Knoxville, TN, USA

Introduction

Powder bed fusion and directed energy deposition are two common additive manufacturing (AM) processes for the fabrication of metals and alloys [1]. These processes involve high temperatures and significant energy, using a laser or electron beam to selectively melt powders that are either pre-deposited to form a powder bed or delivered through feed nozzles [2, 3]. Even with the rapid advances in these beam-based AM processes, there remain challenges such as high energy consumption, material limitations, long processing times, and high costs [4, 5]. To overcome these limitations, solid-state AM processes have been developed that do not rely on beams to melt materials [6–8]. Additive friction stir deposition (AFSD) is one such solid-state AM process that is based on the principles of friction stir welding (FSW). This technique employs a non-consumable rotating tool to produce frictional heat and plastic deformation, enabling metals to be deposited layer by layer onto a substrate [9]. By operating in a solid state, AFSD significantly reduces defects associated with melting and solidification, such as porosity and cracking. This results in highly dense, near-net shape parts [10, 11]. AFSD is particularly beneficial for fabricating or repairing high-strength, heat-sensitive alloys like aluminum, titanium, and steel, which are difficult to process using conventional fusion-based methods [9, 12, 13]. This process has a high degree of tolerance for feed material quality and does not require a fully dense material to produce printed parts, thus allowing for the upcycling of metal waste by converting metallic chips collected from machining operations, shreds from used Al soda cans, and recycled metal matrix composites (MMC) into valuable finished products. By keeping materials in their solid state, AFSD also preserves the original alloy's material properties and prevents grain coarsening, ensuring excellent mechanical performance in the final product. This makes AFSD an attractive option for aerospace, automotive, defense, and marine applications, where material integrity and performance are crucial.

As shown in Fig. 1a, Agrawal et al. [14] explored the impact of processing variables on the microstructure and mechanical properties of Ti6Al4V deposited using AFSD feedstock derived from machining chips. The spindle speed and traverse speed significantly influenced the microstructure and, thus, affected material strength and elongation, as well as tool wear. Machining chips from cast aluminum were ultrasonically cleaned and then cold pressed to produce feedstock for AFSD by Yoder et al. [17]; see Fig. 1b. The strain-hardened deposit showed an increased elongation of 17.8% as compared to 1% in the wrought material. Jordon et al. [15] utilized an auger-based feeding system to directly deposit dry machined aluminum alloy 5083 (AA5083-H131) chips, as shown in Fig. 1c. A fine, equiaxed microstructure was observed and exhibited wrought-like material properties. Beck et al. [16] also deposited solid Al-Mg-Mn alloy (AA5083-H131) and AA5083 feedstock from machining chips to compare the mechanical properties of wrought, solid bar, and recycled feedstock. An increase in both ultimate and fatigue strength for the AFSD recycled chip parts relative to wrought material was observed due to significant grain size reduction.

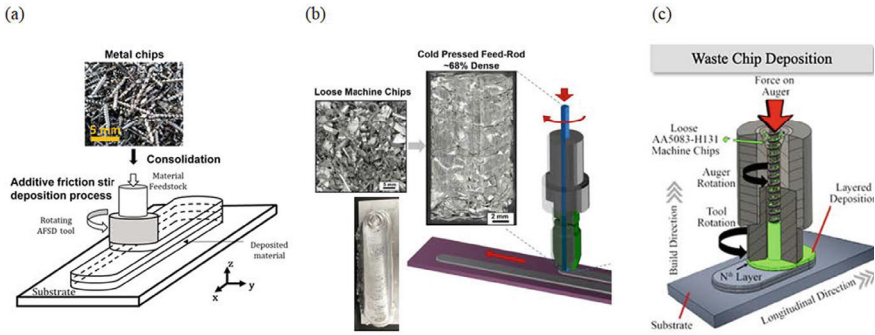


Fig. 1 Additive friction stir deposition of **a** bars from compacted Ti6Al4V machining chips [14], **b** bars from compacted cast Al machining chips [17], and **c** direct recycling of AA 5083 machining chips by feeding through an auger-based system [15]

The recycling of machining chips (or swarf) has also been studied for other AM processes. Sarah et al. [18] explored and established Ti6Al4 swarf as a feasible feedstock material for the laser directed energy deposition (L-DED) process. The microstructure of printed samples varied based on the mechanism of powder formation. Other similar research has shown the successful recycling of steel chips into feedstock powder for printing tracks using L-DED [19, 20]. Rui et al. [21] evaluated the properties of recycled 7075 aluminum alloy obtained as scrap from “aircraft graveyards” to demonstrate good resistance to stress corrosion cracking as well as intergranular corrosion. The authors also highlighted the environmental and industry challenges posed by retiring aircraft and emphasized the need for advanced management solutions.

Chip Compactor Design

This study uses a chip compactor designed and fabricated for use with a hydraulic press. An A2 tool steel ramrod was used to produce 10 cm × 1.27 cm × 1.27 cm Al 6061 feedstock bars. The compactor comprises a ram carriage and a split clamshell-type die set integrated into a 20-ton hydraulic press as shown in the CAD model assembly in Fig. 2a. The ram carriage aligns the ramrod with the die set during the press motion. The carriage assembly includes a ram press adapter, top base, ramrod, and die set. With a fixed top base to minimize deflection, the A2 tool steel ramrod can withstand up to 27 tons of force. The die halves feature a square hole machined to the desired feedstock cross-section of 1.27 × 1.27 cm using wire electric discharge machining (WEDM) and surrounded by three cartridge heater connections, which were then bolted to the bottom base plate. A titanium removal plug, along with titanium washers, isolated the die from the base. Finally, the entire structure, including the ram carriage and die set, was secured in place through a bottom base

and guide rods. To increase throughput by increasing the maximum stroke length of the ramrod, a die extension was 3D-printed and added on top of the dies as shown in Fig. 2b.

To begin compaction, the compactor assembly, shown in Fig. 2a, was mounted and fixed onto the press after aligning the ramrod with the die. Next, aluminum Al 6061 chips were fed into the die and compacted at room temperature by applying a gradually increasing pressure. This step was repeated until the entire length of the bar was compacted. Various chip morphologies, shown in Fig. 3a, b, were tested. Build force was seen to have the maximum impact on the relative density of compacted bars, followed by final force. The force applied during each compaction step and chips fed is defined as the build force here, whereas the final compressive force applied during the last step is the final force. The application of final force is followed by a dwell time during which the ramrod remains inside the die in a state of compaction to limit spring back from the compacted chips. A build force of 6 tons and a final force of 6 tons applied four times were selected as the preferred processing parameters.

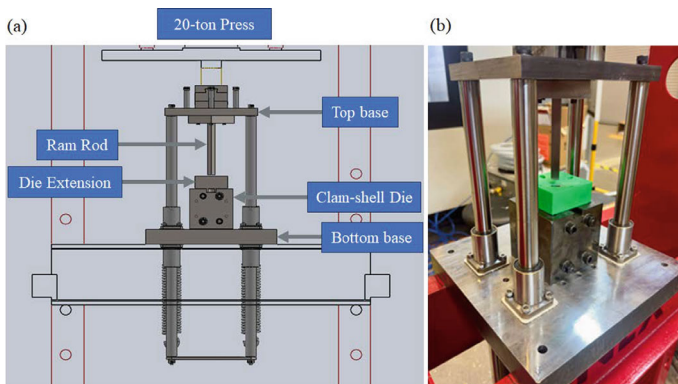


Fig. 2 **a** CAD representation of the chip compactor assembly mounted on the hydraulic press and **b** final chip compactor on press

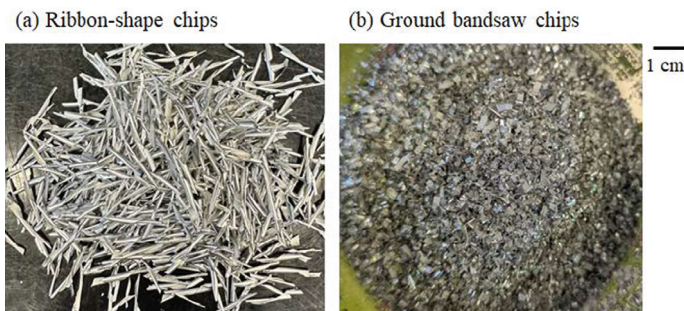


Fig. 3 Various Al 6061 chip morphologies

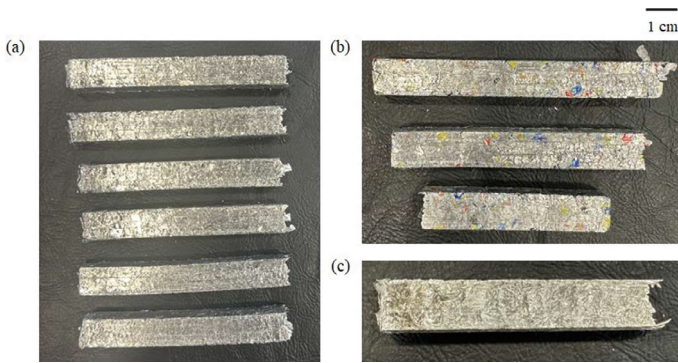


Fig. 4 **a** Consistent Al 6061 ribbon-chip compacted bars with relative densities of 86–100%, **b** shredded Al can, and **c** 25 weight % SiC-Al chip compacted bars

Results and Discussion

Compacted Bars

Initial experiments were conducted using Al 6061 chips produced by milling with a ribbon-like morphology, as shown in Fig. 3a. All chips used for the compaction process were cleaned using an ultrasonic cleaner in an acetone and water bath to remove any residual coolant or impurities. Initial testing gave chunks of compacted chips with relative densities between 21 and 76%. A combination of die design modification and process parameter optimization generated consistent compacted bars of relative densities in the range of 86–100%, as shown in Fig. 4a. Using the same set of parameters, compacted bars were also obtained from shredded Al cans. A mixture of 25% by weight low-cost SiC powder and ribbon-shape Al 6061 chips is shown in Fig. 4b, c. Table 1 shows the measured parameters of mass, volume, density, and relative density for each of these compacted bar materials over a few tests. Note that the relative densities are measured with respect to wrought Al 6061 commercial bars.

Optical Imaging

Samples from the compacted bars were extracted using a precision diamond saw cutter for optical imaging and microscopy. These samples were then mounted onto an epoxy resin before polishing. Polishing was done on a Buehler EcoMet 250 automatic grinder polisher using a 25 N load applied uniaxially and a base rotation speed of 150 rpm coupled with head rotation at 50 rpm. All the samples were prepared using 600 and 1200-grit SiC papers followed by {6, 3, and 1} μm diamond polishing steps

Table 1 Compaction test results

Bar material	Test number	Mass (gm)	Length (cm)	Width x (cm)	Width y (cm)	Volume (cm ³)	Density (gm/cm ³)	Relative density (%)
Machined Al 6061 chips	1	31.7	8.9	1.2	1.2	13.2	2.4	88.9
	2	30.6	8.6	1.2	1.2	12.9	2.4	87.8
	3	32.7	9.2	1.2	1.2	13.3	2.45	90.6
Shredded Al can	1	33.3	9.1	1.22	1.22	13.5	2.47	91.3
	2	35.3	9.5	1.22	1.23	14.4	2.46	90.8
	3	36.4	9.5	1.25	1.24	14.6	2.49	92.2
25% SiC-machined Al chips	1	24	6.6	1.2	1.24	10.1	2.39	88.6
	2	14.8	4	1.2	1.2	5.9	2.5	92.5

in descending order. The optical images were captured on a Nikon Eclipse MA200 inverted microscope using the 5X objective.

Figure 5b–d compares the optical images of ribbon Al-chip bar, shredded Al can bar, and 25 weight % SiC-Al chip composite bar, respectively with wrought Al 6061 commercial bar shown in Fig. 5a. The Al can shreds had a uniform, homogenous, and almost round morphology, which led to lesser voids in the compacted bars as opposed to the machining chip and composite bars. The distribution of the voids within the compacted bar cross-section was seen to follow a pattern similar to the chip morphology itself, which is more elongated and axial for the chip and composite bars as opposed to a meandering pattern for the shredded Al can bars. The SiC particles integrated with the Al chips can be distinctly seen from the darker regions in the corresponding micrograph for the composite bar in Fig. 5d.

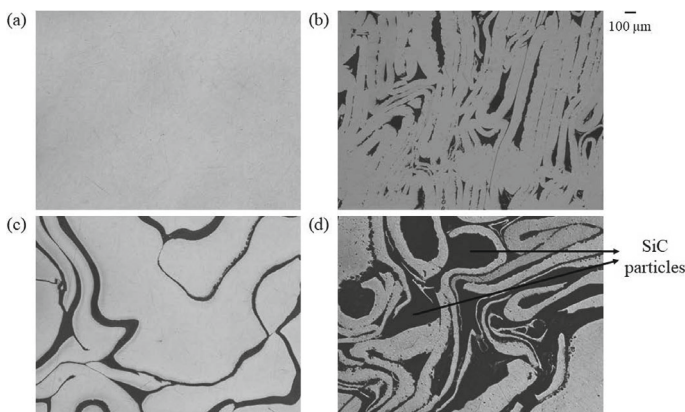


Fig. 5 Optical micrographs of **a** wrought Al 6061 bars, **b** ribbon Al 6061 chip, **c** shredded Al cans, and **d** 25% SiC-Al chip compacted bars

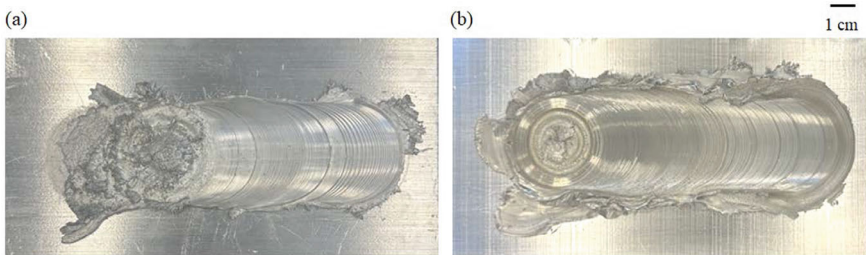


Fig. 6 Printed **a** Al 6061 chip bars incorporating commercial 6061 “cheater” bars and **b** shredded Al can bars using additive friction stir deposition (AFSD)

Table 2 Initial AFSD printing parameters

Print parameters	Value
Spindle speed (N)	325–400 rpm
Traverse speed (V)	15.2–25.4 mm/min
Actuator feed rate (f)	12.7–25.4 mm/min
Layer height (h)	0.8 mm
Tool material	H13 Steel

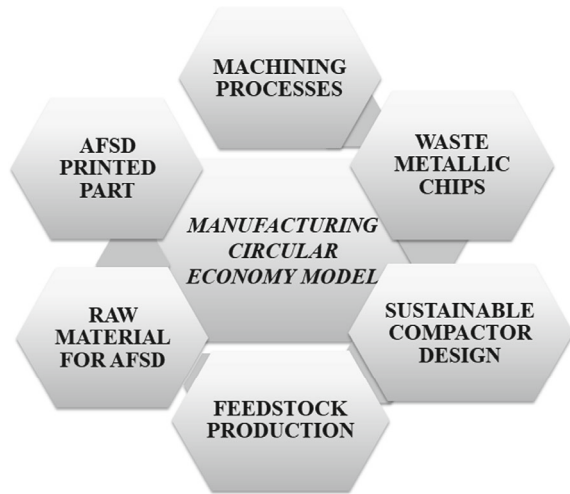
Additive Friction Stir Deposition

Printing of compacted bars was performed on a MELD Manufacturing L3 machine [9]. Initial process parameters were set as shown in Table 2. These preliminary tests using AFSD gave significant flash and poor deposited material consolidation. To overcome this and to ensure material deposition on the base plate without delamination, a small section of commercial Al 6061 “cheater” bar was incorporated into the printing process for depositing the 6061 chip bars, as shown in Fig. 6a. The deposition was initiated using the wrought feedstock, and this initial bar was backed by the compacted bars. The shredded Al can bars printed three layers successfully, see Fig. 6b. To obtain consistent deposits using the compacted bars, the process parameters of spindle rotation, traverse speed, material feed rate, and layer height must be adjusted relative to wrought bars. This testing is in progress.

Conclusion

Due to severe plastic deformation and material stirring enabled by frictional heat from a rotating tool, AFSD not only provides material consolidation in a solid state but also alters the microstructure while avoiding cracks, porosity, and defects. The outcome is wrought-like mechanical properties with a homogenous microstructure. AFSD is a suitable solid-state AM process for upcycling machined metallic chips, aluminum can

Fig. 7 Circular economy model using machining chips for recycled feedstock production



scrap, and recycled composite material to use as feed materials in the fabrication of 3D preforms. In contrast, fusion-based aluminum recycling offers limited upcycling benefits due to significant alteration in the resulting material microstructure and mechanical properties.

The chip compactor system design presented in this work is engineered to recycle and repurpose machining chips, shredded aluminum cans, and low-cost SiC-aluminum chip metal matrix composites into feedstock material for AFSD processes. The compactor assembly incorporates a die set and ram carriage onto a hydraulic press to produce compacted bars under cold (room temperature) and warm (elevated temperature) working conditions using compressive mechanical forces and integrated cartridge heaters. Using this chip compactor, bars of relative densities ranging from 86 to 100% (fully dense) have been successfully produced. Since the compacted bars undergo severe plastic deformation without melting during the AFSD process, achieving 100% relative density is not critical for operation. The relative densities achieved were seen to be moderately influenced by the morphology of the compacted material. Three layers of the compacted aluminum machining chips and shredded aluminum can bars were deposited using AFSD. Current and future work will include optimizing the printing process parameters, including deposition temperature, spindle speed, traverse speed, material feed rate, and layer height, to produce consistent deposits with desired mechanical properties.

The potential of AFSD to advance circular economy principles and materials sustainability presents a significant opportunity. The broader goal of this research is to improve sustainability within AFSD and support the adoption of a circular economy model in additive manufacturing, as shown in Fig. 7.

References

1. ASTM F2792 (2015) Standard terminologies for additive manufacturing technologies ASTM International
2. Carroll BE, Palmer TA, Beese AM (2015) Anisotropic tensile behavior of Ti–6Al–4V components fabricated with directed energy deposition additive manufacturing. *Acta Mater* 87:309–320. <https://doi.org/10.1016/j.actamat.2014.12.054>
3. King WE, Anderson AT, Ferencz RM, Hodge NE, Kamath C, Khairallah SA, Rubenchik AM (2015) Laser powder bed fusion additive manufacturing of metals; physics, computational, and materials challenges. *Appl Phys Rev* 2(4):041304. <https://doi.org/10.1063/1.4937809>
4. Martin JH, Yahata BD, Hundley JM, Mayer JA, Schaedler TA, Pollock TM (2017) 3D printing of high-strength aluminium alloys. *Nature* 549(7672):365–369. <https://doi.org/10.1038/nature23894>
5. Murr LE, Gaytan SM, Ramirez DA, Martinez E, Hernandez J, Amato KN, Shindo PW, Medina FR, Wicker RB (2012) Metal fabrication by additive manufacturing using laser and electron beam melting technologies. *J Mater Sci Tech* 28(1):1–14. [https://doi.org/10.1016/S1005-0302\(12\)60016-4](https://doi.org/10.1016/S1005-0302(12)60016-4)
6. Kong C, Soar R, Dickens P (2003) Characterization of aluminium alloy 6061 for the ultrasonic consolidation process. *Mater Sci Engg A* 363(1–2):99–106. [https://doi.org/10.1016/S0921-5093\(03\)00590-2](https://doi.org/10.1016/S0921-5093(03)00590-2)
7. Palanivel S, Nelaturu P, Glass B, Mishra R (2015) Friction stir additive manufacturing for high structural performance through microstructural control in an Mg based WE43 alloy. *Mater Des* 65:934–952. <https://doi.org/10.1016/j.matdes.2014.09.082>
8. White D (2002) Object consolidation employing friction joining. US Patent 6,457,629
9. MELD Brochure—Aeroprobe Corporation (2018). <http://www.aeroprobe.com/meld/>
10. Yu HZ, Jones ME, Brady GW, Griffiths RJ, Garcia D, Rauch HA, Cox CD, Hardwick N (2018) Non-beam-based metal additive manufacturing enabled by additive friction stir deposition. *Scripta Materialia* 153:122–130. <https://doi.org/10.1016/j.scriptamat.2018.03.025>
11. Yu HZ, Mishra RS (2020) Additive friction stir deposition: a deformation processing route to metal additive manufacturing. *Mater Res Lett* 9(2):71–83. <https://doi.org/10.1080/21663831.2020.1847211>
12. Schultz JP, Kevin C (2014) Friction stir fabrication. US Patent 8,636,194
13. Palanivel S, Mishra RS (2017) Building without melting: a short review of friction-based additive manufacturing techniques. *Int J Add Subtr Mater Manuf* 1(1):82–103. <https://doi.org/10.1504/IJASMM.2017.082991>
14. Agrawal P, Haridas RS, Yadav S, Thapliyal S, Gaddam S, Verma R, Mishra RS (2021) Processing-structure-property correlation in additive friction stir deposited Ti-6Al-4V alloy from recycled metal chips. *Add Manuf* 47:102259. <https://doi.org/10.1016/j.addma.2021.102259>
15. Jordon J, Allison P, Phillips B, Avery D, Kinser R, Brewer L, Cox C, Doherty K (2020) Direct recycling of machine chips through a novel solid-state additive manufacturing process. *Mater Des* 193:108850. <https://doi.org/10.1016/j.matdes.2020.108850>
16. Beck S, Williamson C, Kinser R, Rutherford B, Williams M, Phillips B, Doherty K, Allison P, Jordon J (2023) Examination of microstructure and mechanical properties of direct additive recycling for Al-Mg-Mn alloy Machine chip waste. *Mater Des* 228:111733. <https://doi.org/10.1016/j.matdes.2023.111733>
17. Yoder JK, Hahn GD, Zhao N, Brennan RE, Cho K, Yu HZ (2023) Additive friction stir deposition-enabled upcycling of automotive cast aluminum chips. *Add Manuf Lett* 4:100108. <https://doi.org/10.1016/j.addlet.2022.100108>
18. Wolff S, Haddad M, Zhang J, Luo A (2024) Effect of recycled swarf and spherical Ti-6Al-4V feedstocks on laser directed energy deposition additive manufacturing. *CIRP Ann.* <https://doi.org/10.1016/j.cirp.2024.03.013>

19. Fullenwider B, Kiani P, Schoenung JM, Ma K (2019) Two-stage ball milling of recycled machining chips to create an alternative feedstock powder for metal additive manufacturing. *Powder Tech* 342:562–571. <https://doi.org/10.1016/j.powtec.2018.10.023>
20. Jackson MA, Morrow JD, Thoma DJ, Pfefferkorn FE (2020) A comparison of 316 L stainless steel parts manufactured by directed energy deposition using gas-atomized and mechanically-generated feedstock. *CIRP Ann* 69(1):165–168. <https://doi.org/10.1016/j.cirp.2020.04.042>
21. Lin R, Liu B, Zhang J, Zhang S (2022) Microstructure evolution and properties of 7075 aluminum alloy recycled from scrap aircraft aluminum alloys. *J Mater Res Tech* 19:354–367. <https://doi.org/10.1016/j.jmrt.2022.05.011>